Absence of cardiolipin from the mitochondrial inner membrane outer leaflet restricts Opa1-mediated fusion

Yifan Ge[1,2,*,^], Sivakumar Boopathy[1,2], Tran H Nguyen[1,2], Camila Makhlouta Lugo[1,2], Luke H. Chao[1,2,^]

1. Department of Molecular Biology, Massachusetts General Hospital, Boston, Massachusetts, U.S.A, 02114
2. Department of Genetics, Harvard Medical School, Boston, Massachusetts, U.S.A.

*Current address: Key Laboratory of Neuroregeneration of Jiangsu and the Ministry of Education, Nantong University, Nantong, Jiangsu, China.

^ Two whom correspondence should be addressed

Abstract

Cardiolipin is a tetra-acylated di-phosphatidylglycerol lipid enriched in the matrix facing (inner) leaflet of the mitochondrial inner membrane. Cardiolipin plays an important role in regulating mitochondria function and dynamics. Yet, the mechanisms connecting cardiolipin distribution and mitochondrial protein function remain indirect. In our previous work, we established an *in vitro* system reconstituting mitochondrial inner membrane fusion mediated by Opa1. We found that the long form of Opa1 (l-Opa1) works together with the proteolytically processed short form (s-Opa1) to mediate fast and efficient membrane fusion. Here, we extend our reconstitution system to generate supported lipid bilayers with asymmetric CL distribution. Using this system, we find the presence of CL on the intermembrane space-facing (outer) leaflet is important for membrane tethering and fusion. We discuss how the presence of CL in this leaflet may influence protein and membrane properties, and future applications for this approach.

Introduction

Mitochondria are important eukaryotic organelles that regulate cell metabolism, signaling and death (McBride et al., 2006;Giacomello et al., 2020). Mitochondria feature a unique double membrane structure. The outer mitochondrial membrane (OMM) hosts machinery for lipid and protein transport, while the inner mitochondrial membrane (IMM) is the site for ATP synthesis, and respiratory chain complexes (Kroemer et al., 2007). Cristae, the membrane invaginations of the inner membrane, are important for respiratory function (Cogliati et al., 2016;Kondadi et al., 2020). Mitochondrial membranes are dynamic, undergoing fusion and fission to distribute metabolites and buffer mutation in mitochondrial DNA, while changing morphology in response to physiological conditions (Chan, 2020;Gao and Hu, 2021).

While phospholipid composition is recognized as a key regulator of membrane properties, the functional roles of phospholipid distribution are challenging to investigate (Harayama and Riezman, 2018). The mitochondrial membrane is distinct in composition from other

endomembrane systems, and comprises cardiolipin (CL), phosphocholine (PC), and phosphatidylethanolamine (PE) (Horvath and Daum, 2013). Other species, which may play important roles include phosphatidylinositol (PI), phosphatidylserine (PS), phosphatidylglycerol (PG), phosphatidic acid (PA), lysophospholipids, sterols, sphingomyelin and low levels of cholesterol (CH) (Horvath and Daum, 2013).

In eukaryotes, CL is uniquely found in the mitochondria. Consistent with an endosymbiotic origin, CL is found in bacteria (Friedman and Nunnari, 2014). In eukaryotes, CL comprises ~20% of total mitochondrial phospholipid content. In the OMM, PC and PE are major membrane components. In contrast, PE and CL makes up nearly 50% of the total phospholipid in the IMM (Horvath and Daum, 2013;Oemer et al., 2018;Oemer et al., 2020). Spectroscopic and fluorescence studies indicate CL enrichment in the matrix-facing (inner) leaflet of the IMM (Kagan et al., 2014). Electron paramagnetic resonance spectroscopy studies of yeast mitochondria also show CL enrichment in the inner leaflet of the IMM (Petit et al., 1994). An inner leaflet IMM distribution of CL was shown using fluorescent probes that specifically target CL (Krebs et al., 1979;Harb et al., 1981;Petit et al., 1994). These observations are consistent with data indicating CL is synthesized from PA in the matrix proximal face of the IMM (Schlame, 2008). While the distribution between leaflets may be dynamic, data suggest CL also comprises ~5-15% of the total lipids in the IMS-facing (outer) leaflet (Harb et al., 1981;Gallet et al., 1997).

CL has four acyl chains, forming a unique conical structure expected to have high flexibility. This structure classifies CL as a ‘non-structural’ phospholipid that tends to introduce a hexagonal phase in mixtures (Kagan et al., 2014). The high concentration of PE and CL in the IMM is expected to alter membrane tension (Traïkia et al., 2002), which influences membrane bending. Differential stress between leaflets can change membrane elasticity, stiffness and lateral pressure (Hossein and Deserno, 2020). These changes can favor incorporation of transmembrane proteins that induce curvature, association of peripheral membrane proteins, or self-assembly of proteins on either leaflet (Wilson et al., 2019;Lorent et al., 2020).

In addition to inter leaflet asymmetry, lipids can exhibit planar segregation (Doktorova et al., 2020;Lorent et al., 2020). Planar segregation in the plasma membrane has been more extensively studied (Lorent et al., 2020). For example, model plasma membrane experiments show planar segregation coupled with inter leaflet asymmetry can affect lipid packing and hydrophobic thickness, to sequester transmembrane proteins (Hussain et al., 2013). Similar physical consequences of planar segregation may be at play in the IMM. For example, cellular experiments suggest membrane heterogeneity may play a role in organizing respiratory chain super complexes (Dudek, 2017).

Theoretical and computational approaches have also investigated the physical effects of CL distribution heterogeneity (Lemmin et al., 2013;Boyd et al., 2017;Elias-Wolff et al., 2019;Wilson et al., 2019). Not surprisingly, CL distribution is predicted to strongly shape the electrostatic potential of membrane surface, with cation interactions observed to introduce lateral CL heterogeneity in simulations. (Lemmin et al., 2013). Boyd and coworkers show concentration-dependent bending and buckling of CL bilayers, with CL mediating regions of high curvature, and CL concentrating in the negatively curved regions (Boyd et al., 2017). This finding was

supported by work from Elias-Wolf and coworkers, which also found CL inter-leaflet asymmetry contributes to membrane buckling (Elias-Wolff et al., 2019).

CL distribution changes in response to environmental stimuli and has important consequences in disease (Gallet et al., 1997). Recent studies show CL can be externalized by pro-mitophagy stimuli in primary cortical neurons and in Parkinson's Disease cellular models (Chu et al., 2013). Externalization of CL to the outer leaflet of the OMM activates binding to microtubule-associated-protein-1 light chain 3, which localizes damaged mitochondria to autophagosomes (Chu et al., 2013;Ryan et al., 2018). CL externalization is recognized by macrophages to cause inflammation (Pizzuto and Pelegrin, 2020). These processes are associated with altered fission and fusion dynamics and altered mitochondrial morphology (Kordower et al., 2008;Van Laar and Berman, 2009). Many mitochondrial proteins depend on CL for activity (Ban et al., 2010;Zhang et al., 2020), yet the role of asymmetric lipid distribution on protein activity has been technically challenging to investigate.

In our previous work, we fabricated a model membrane system that mimicked the mitochondrial inner membrane in composition. We reconstituted Opa1 (the IMM fusogen) into a supported bilayer and noticed CL played a key role in several stages of membrane fusion (in particular, GTP-dependent membrane tethering). In our previous study, we focused on understanding how the full length 'long form' of l-Opa1 worked together with a proteolytically processed 'short form' (s-Opa1) to regulate full fusion. We showed that while l-Opa1 can induce low levels of membrane fusion, both s-Opa1 and l-Opa1 are required for fast and efficient fusion. These experiments were performed under conditions containing symmetric lipid composition in the bilayer, with both leaflets containing 20% CL. In these previous experiments, we found that when the model membranes lacked CL entirely, fusion was rare.

Here, we present new data investigating Opa1 activity under asymmetric bilayer conditions. We take advantage of our synthetic model-membrane system to generate supported lipid bilayers with no CL in the outer-leaflet, and CL in the inner-leaflet. Our new results show CL in the outer leaflet (facing the IMS) plays an important role in Opa1-mediated bilayer tethering and pore opening. These data implicate CL-protein interactions during specific steps of membrane fusion. We discuss how changes in bilayer composition may influence membrane properties and protein-protein interactions.

Materials and Methods

Preparation of polymer-tethered asymmetric bilayers and reconstitution of l-Opa1 into asymmetric bilayers

Polymer tethered lipid bilayers were fabricated using mixtures of synthesized lipid reagents, including 1,2-dioleoyl-sn-glycero-2-phosphocholine, (DOPC); 1,2-dioleoyl-sn-glycero-2-phosphoethannolamine-N-[metoxy(polyethylene glycerol)-2000] (DOPE-PEG2000), L-α-phoshphatidylinositol (liver PI) and 1',3'-bis[1,2-dioleoyl-sn-glycero-3-phospho]-glycerol (18:1 cardiolipin) from Avanti Polar Lipids (AL, USA). Inter leaflet asymmetric bilayers were assembled in a layer-by-layer manner, using a combination of Langmuir-Blodgett dipping and Langmuir-Schaefer transfer. Bilayers were fabricated on a glass substrate (25 mm diameter cover

glass, Fisher Scientific) as previously described (Ge et al., 2020b). For all fusion experiments, the bottom leaflet included 7 %(mol) liver PI, 20 %(mol) CL, 20 %(mol) DOPE, 0.2 %(mol) Cy5-PE and 5 %(mol) DOPE-PEG2000. For fluorescent anisotropy analysis, the bottom leaflet contained 0.2 %(mol) Top-fluor CL (Avanti Polar Lipids), which served as a reporter for CL distribution and means to evaluate lipid flip-flop. The lipid mixture was spread carefully on top of the air-water interface on a Langmuir-Blodgett trough (KSV-NIMA, NY, USA). A film was applied at a pressure of 37 mN/m and kept for 30 mins., then transferred to the glass substrate, forming the bottom leaflet of the bilayer. For l-Opa1 reconstitution experiments, the top leaflet (mimicking the outer, IMS-facing side) of the asymmetric bilayer was completely CL free, whereas the bottom leaflet (facing the inner, matrix side) contains 20% CL. Cy5-PE was used to monitor fusion kinetics. For all bilayers, the lipid mixture of the bottom leaflet was spread on top of the air-water interface, while pressure was kept at 37 mN/m for 30 mins before dipping. The bottom leaflet was prepared at 30 mN/m pressured for 30 mins before Schaefer transfer and assembly into an asymmetric bilayer. This helped maintain a similar area/molecule ratio in both top and bottom leaflets (Ge et al., 2020b).

Purification and reconstitution of Opa1 in asymmetric bilayers

l- and s-Opa1 were purified following a protocol reported previously (Ge et al., 2020a;Ge et al., 2020b). Human l-Opa1 (isoform 1) and s-Opa1 with Twin-strep-tag at N-terminus and deca-histindine tag at C-terminus (GenScript, NJ, USA) was expressed in *Pichia pastoris* strain SMD1163. The cells were harvested and milled using SPEX 6875D Freezer/Mill. The milled powder was resuspended in buffer containing 50 mM sodium phosphate, 300 mM NaCl, 1 mM 2-mercaptoethanol, pH 7.5, with benzonase nuclease and protease inhibitors. The membrane fraction was collected by ultra-centrifugation at 235,000 xg for 45 min. at 4 °C, then incubated for 1 hour in the same resuspension buffer supplemented with 2 % DDM (Anatrace, OH, USA) and 0.1 mg/ml cardioipin. Membrane fraction solubilized in DDM containing buffer was ultracentrifugated at 100,000 x g for 1 hour at 4 °C. The supernatant extract containing l-Opa1 was loaded onto a Ni-NTA column (Biorad, CA, USA), washed with 50 mM sodium phosphate, 350 mM NaCl, 1 mM 2-mercaptoethanol, 1 mM DDM, 0.025 mg/ml 18:1 CL, pH 7.5, with 25 mM imidazole followed with 100 mM imidazole. The bound Opa1 was eluted with the above buffer containing 500 mM imidazole. The elution was buffer exchanged into 100 mM Tris-HCl, 150 mM NaCl, 1 mM EDTA, 1 mM 2-mercaptoethanol, 0.15 mM DDM, 0.025 mg/ml 18:1 CL, pH 8.0. The C-terminal His-tag was then cleaved by treatment with TEV protease and further purified with Strep-Tactin XT Superflow column (IBA life Sciences, Göttingen, Germany). The tandem-affinity tagged protein was detached from Strep-Tactin XT column was detached and eluted with buffer containing 50 mM biotin. The elution fraction was concentrated and subjected to size exclusion chromography in buffer with 25 mM Bis-tris Propane, 100 mM NaCl, 1 mM TCEP, 0.025 mg/ml 18:1 CL, pH 7.5.

l-Opa1 was reconstituted by mixing purified l-Opa1 with a surfactant cocktail containing DDM and OG, applied as reconstitution reagents, at a concentration of 1.2 nM and 1.1 nM, respectively. l-Opa1 was reconstituted to total amount of 1.3×10^{-12} mol (protein:lipid 1:100000). The protein was incubated for 2 hrs in surfactant at room temperature. Extra surfactant was then removed using Bio-Beads SM2 (Bio-Rad, CA, USA), at a concentration of 10 µg/ml.

Preparation of liposomes and proteoliposomes

Calcein encapsulated liposomes containing 7 %(mol), PI 20 %(mol), CL, 20 PE % (mol), 0.2 %(mol), TexasRed-PE, and DOPC 52.8 %(mol), were prepared as previously described. Lipids dissolved chloroform were mixed in the approproiate ratio and dried under nitrogen flow for 20-30 mins. The resulting lipid film was hydrated with calcein containing Bis-Tris buffer (50 mM calcein, 25 mM Bis-Tris, 150 mM NaCl, pH 7.4) at 70 °C for 30 mins following vigorous agitation. The resulting vesicles were homogenized using a mini-extruder using 200 nm polycarbonate membrane for 15-20 times extrusion to prepare large unilamellar vesicles (LUVs).

l-Opa1 was reconstituted in the LUVs at a molar ratio of 1:5000. Purified l-Opa1 was added to the LUV suspensions with DDM (final concentration 0.1 µM) and incubated for 2 hours at 4 °C. After reconstitution, the sample was dialyzed against calcein buffer using a 3.5 kDa dialysis cassette at 4 °C overnight. Calcein that was not encapsulated in the liposomes were removed using a PD10 desalting column.

TIRF microscopy and fluorescent anisotropy analysis

Fluorescent images are taken using a Vector TIRF system (Intelligent Imaging Innovation, Inc, Denver, CO, USA) equipped with a W-view Gemini system (Hamamatsu photonics, Bridgewater, NJ). TIRF images were acquired using a 100X oil-immersion TIRF objective (Zeiss, N.A 1.4). Fluorescent images were taken using a Prime 95B scientific CMOS camera kept at -10 °C (Photometrics), recorded at a frame rate of 100 ms.

To validate bilayer asymmetry, fluorescent anisotropy was measured using a modified light path embedded in the microscopy. Under this experimental setting, the 488 nm excitation laser was polarized through a fiber switch system, equipped with internalized polarizer (Intelligent Imaging Innovation, Inc, Denver, CO, USA). The p- and s- emission were separated using a polarized beam splitter (532 nm, Thorlabs) inserted in the Gemini system. As a result, p-emission and s-emission was separated onto two halves of the camera chip. To ensure a reliable emission result, the p-polarized emission and s-polarized emission was adjusted to be similar intensity and was determined using a photometer. The fluorescent anisotropy of dye-labeled bilayers in both symmetric and asymmetric bilayers was determined by the following formula:

$$r = \frac{I_{\perp} - GI_{\parallel}}{I_{\perp} + 2GI_{\parallel}}$$

Where G represents the correction factor (added to compensate for uneven light distribution caused by the polarized emission beam splitter optics, and potential depolarization effects caused by the high NA objective). The G factor was determined using a sample solution containing 1 mM calcein dissolved in glycerol, where the fluorescent anisotropy was well defined. The G factor was evaluated for each pixel of the image before every measurement, and the final *r* of each pixel was obtained and averaged for the lipid bilayer samples to eliminate potential effects of inner leaflet dye aggregation.

For fusion and membrane tethering experiments, a 543 nm laser was used to analyze TexasRed-PE signal in liposomes and proteoliposomes and to observe lipid demixing. The bilayer was labeled with Cy5 (excited by a 633 nm laser), that reported on homogeneity of the bilayer. A 488 nm laser was applied for recording content release of the encapsulated calcein. Time-lapse images were taken at a frequency of 100 ms to record fusion dynamics.

Results

Bilayers with asymmetric cardiolipin distribution can be generated through layer-by-layer assembly

We generated a PEG polymer-tethered lipid bilayer with asymmetric CL distribution that mimics the leaflet distribution found in the mitochondrial inner membrane. Our approach was inspired by methods successfully used to study the leaflet asymmetry of cholesterol in the plasma membrane (Hussain et al., 2013). These methods have been used to study phase separation in planar lipid bilayers and liposomes (Hussain et al., 2013;Doktorova et al., 2018;London, 2019). Our control symmetric bilayers comprised 15 %(mol) CL on both top and bottom leaflets (with 0.1 % CL in both leaflets replaced by Top-Fluor CL) (Fig 1A). Control asymmetric bilayers comprised 10 %(mol) CL on the top leaflet and 20 %(mol) CL in the bottom leaflet (Top-Fluor CL only labeling the bottom leaflet). We noticed symmetric bilayers fabricated in our previous work had to be used immediately, as they acquired defects within 24 hours (Ge et al., 2020b). We did not observe this issue with our asymmetric bilayers, which were stable for at least 48 hours.

We analyzed TIRF-based fluorescent anisotropy images to evaluate lipid asymmetry, as performed previously in cellular membrane and model liposome membranes (Li et al., 2019;St Clair et al., 2020). Both symmetric and asymmetric bilayer were labeled with the same total concentration of fluorophore. EPI-fluorescence images show the same fluorescent intensity (Fig 1B and E). Fluorescence anisotropy of the asymmetric bilayer (average r_{asy} = 0.125) was approximately four times higher than that of the symmetric bilayer (average r_{sym} = 0.024) (Fig 1G). Models of plasma membrane asymmetry show high levels of cholesterol and phospholipid scrambling, which causes membranes to homogenize over time (Doktorova et al., 2020). To evaluate the potential for CL flip-flop and loss of bilayer asymmetry anisotropy measurements were also performed after 24 and 48 hours. There was no statistically significant anisotropy change after 48 hours at 4 °C. These findings are consistent with simulation studies showing that an asymmetric distribution of CL is thermodynamically favorable (Kagan et al., 2015;Elias-Wolff et al., 2019).

l-Opa1 mediated homotypic membrane tethering is dependent on CL in the outer leaflet

In our previous studies, we showed CL is important for both l-Opa1 (homotypic and heterotypic) and s-Opa1-mediated membrane tethering (Ge et al., 2020b). l-Opa1 tethering can potentially occur through homotypic protein-protein interactions, or heterotypic protein-lipid interactions. Here, we first investigated homotypic l-Opa1 membrane tethering in a bilayer with asymmetric CL distribution. We compared four conditions varying CL presence in the bilayer and proteoliposome. Initial validation of our system show that we can generate asymmetric bilayers

that are stable even with 10% inter-leaflet difference in CL concentration. To evaluate Opa1 function under extreme membrane asymmetry, we completely depleted the CL on the top leaflet in our reconstitution experiments, while leaving 20% CL in the bottom leaflet. We found that with these asymmetric bilayers, under homotypic l-Opa1 conditions (reconstituted in both bilayer and liposome), the presence of CL does not significantly stimulate GTP-independent membrane tethering, independent of the location of CL or leaflet distribution (Fig 2 A-ii apo, A-iv apo).

Our previous data, and observations from others (Ban et al., 2010), show that membrane embedded CL can mediate nucleotide-dependent membrane tethering. Interestingly, we observe reduced particle tethering when CL was asymmetrically distributed (CL absent from the top leaflet of the planar bilayer), compared to the symmetrically distributed case (Fig 2A iii and iv). Our quantification shows that when CL is present in both leaflets of the bilayer (regardless of the CL content in proteoliposomes), addition of GTP induces ~three-fold more proteoliposome tethering to the bilayer (Fig 2B, 2A ii and iv). In contrast, when CL is depleted from only the outer leaflet of the bilayer, GTP is only able to trigger ~1.5 fold-more proteoliposomes tethering to the bilayer (Fig 2 A iii).

s-Opa1 promotes membrane tethering in asymmetric CL bilayers.

Proteolytic processing of the transmembrane anchored l-Opa1 to s-Opa1 is a key cellular regulator of mitochondrial inner membrane fusion and cristae state (Del Dotto et al., 2017;Wang et al., 2021) Our previous *in vitro* reconstitution studies using symmetric membranes, showed that stoichiometric levels of s-Opa1 were optimal for stimulating fast and efficient membrane fusion by l-Opa1(Ge et al., 2020b). This helped reconcile observed cellular effects on mitochondrial reticulum phenotypes when modulating the fusion-fission equilibrium (Song et al., 2007;Ehses et al., 2009;Anand et al., 2014;Wang et al., 2021). Here, we investigate the effect of s-Opa1 addition in an asymmetric CL bilayer system. Unexpectedly, depleting CL from the top leaflet of the supported planar bilayer changed the effect of s-Opa1 on proteoliposome tethering.

Upon addition of s-Opa1 at a sub-stoichiometric ratio of 1:10 s-Opa1:l-Opa1, the number of tethered proteoliposomes increased >5 fold (Fig 3B). Addition of stoichiometric levels of s-Opa1 to l-Opa1, did not increase proteoliposome tethering to the bilayer. Instead, lipid tubes were observed to form. These tubes were tethered to the bilayer. When s-Opa1 levels were in excess of l-Opa1, fewer proteoliposomes were observed tethered to the bilayer, and the lipid tubes dissociated from the bilayer surface (Fig 3D and E).

Outer leaflet cardiolipin plays roles in efficient l-Opa1-mediated homotypic fusion and s-Opa1 stimulated fusion

Model membrane and cellular studies show l-Opa1 is required for membrane fusion, and s-Opa1 plays an important stimulatory role (Song et al., 2007;Ge et al., 2020b). Previously, we developed three color imaging assay to evaluate the kinetics of membrane fusion. Briefly, membrane docking was defined by the FRET signal between Cy-5 (bilayer label) and TexsasRed (proteoliposome label). Lipid demixing or hemifusion events were reported by a proteoliposome marker (TexasRed) diffusing into the lipid bilayer. And release of calcein from the proteoliposomes (loaded at quenched concentrations) reported on pore opening events and their

kinetics. Using this assay, we observed low levels of hemifusion and full fusion (pore opening) in a homotypic l-Opa1 format (l-Opa1 reconstituted into the supported bilayer and proteoliposomes, both with symmetric CL distribution). Under these conditions, addition of s-Opa1 dramatically stimulated full fusion.

Here, we find l-Opa1 reconstituted bilayers with asymmetric CL distribution, fewer hemifusion events (Figure 4D, G) compared to our previous finding in symmetric bilayers (Ge et al., 2020b) In contrast, under symmetric cardiolipin conditions, 20% of the total particles are hemifused to the bilayer. Under asymmetric conditions, addition of s-Opa1 also did not increase the efficiency of membrane hemifusion or fusion (Figure 4D, G).

We also observed a significant delay in lipid demixing with l-Opa1 alone. Compared to symmetric bilayers, the average time for lipid demixing in asymmetric bilayers changed from 15 s to 20 s (in the ~50 events calculated in 3 different experiments) (Figure 4B, C), whereas the content release time changed from 20 s to 30 s or more (Figure 4E, F). The calcein release time was also significantly longer (from milliseconds to several seconds) with asymmetric CL bilayers, possibly suggesting an effect on calcein diffusion due to slow fusion pore expansion. Together these observations all point to the importance of CL in the outer, IMS-facing leaflet in efficient s-Opa1 stimulated fusion.

Discussion

The mitochondrial inner membrane (IMM) is expected to have an asymmetric distribution of CL under physiological conditions (Kagan et al., 2014;Pizzuto and Pelegrin, 2020). In this study, we used an *in vitro* model IMM to explore Opa1 activity upon selectively depleting CL from the outer leaflet. We found three interesting effects under these asymmetric CL conditions. First, removing CL from the outer-leaflet reduces GTP-dependent homotypic l-Opa1 tethering. Second, we observe lipid tube formation when sub-stoichiometric levels of s-Opa1 are added l-Opa1 tethered liposomes. Third, asymmetric CL distribution slows pore opening kinetics. These observations all point the importance of CL in the outer-leaflet in mediating efficient fusion.

Recent structures of s-Opa1 and its yeast orthologue s-Mgm provide candidate interfaces for understanding self-assembly. These structures all show Opa1 with a canonical dynamin-family GTPase domain arrangement, with GTPase domain, bundle signaling element (BSE), stalk domain and paddle region (Faelber et al., 2019;Zhang et al., 2020). Basic and hydrophobic residues in the paddle region directly interact with membranes containing CL (Faelber et al., 2019;Yan et al., 2020;Zhang et al., 2020). Mutation of these residues results in decreased affinity of s-Opa1 to the lipid bilayer and affects GTPase activity (Zhang et al., 2020). In Cryo-ET studies, interfaces mediated through the helical stalk region mediate self-assembly(Faelber et al., 2019).

Our observation of reduced tethering under asymmetric conditions suggests that the presence of CL in the outer leaflet facilities inter membrane interactions. We still lack high-resolution structural information for l-Opa1. Existing observations suggest potential modes of CL-influenced tethering may be at play. First, CL may directly stabilize a conformation of Opa1 such that it can interact in a homotypic fashion with another copy of Opa1 in the proteoliposome

bilayer. Second, Opa1 in the proteoliposome bilayer may interact with CL in the supported bilayer. Our results are unable to discriminate between these two non-exclusive modes of interaction. It should be noted, that although the outer leaflet of the bilayer was fabricated without CL for our assay, recombinant l-Opa1 was purified in the presence of CL. We estimate that during reconstitution, around 10^{-12} mol of CL may be reconstituted into the outer leaflet, resulting in an outer leaflet with 0.01 %(mol) CL. Based on previous GTP-assays, this level of cardiolipin is unlikely to be significant in affecting Opa1 activity(Ge et al., 2020b). In this work, we did not explore conditions with ~5-10% CL in the outer leaflet. The details of these asymmetric conditions may be an area for fruitful future investigation.

In our previous work with symmetric bilayers, we did not observe lipid tube formation under the protein concentrations used (Ge et al., 2020b). Interestingly, we do observe tubes in the asymmetric bilayer system used in this study upon addition of s-Opa1. In this work (and our previous studies), we used low concentrations of reconstituted protein in the bilayers and liposomes (total l-Opa1 concentration of 6.5×10^{-12} mol/ml (protein:lipid, 1:5000), and a final s-Opa1 concentration of 6.5×10^{-11} mol/ml, (final protein:lipid 1:500) (Ge et al., 2020b). Membrane tubes are an intriguing *in vitro* observation of Opa1 behavior, with several candidate *in vivo* roles proposed. The Daumke and Sun groups determined helical assemblies of s-Mgm1 and s-Opa1 decorating the outside of lipid tubes, inducing positive curvature (Faelber et al., 2019;Zhang et al., 2020). Faelber and colleagues also observe s-Mgm1 tubes decorating the interior of tubes, with negative curvature (analogous to the topology expected within cristae). Li and co-works suggest a s-Mgm1 trimer may help 'bud' regions of bilayer, through puckering membrane with positive curvature (Yan et al., 2020). In these reports, s-Opa1 was added at 1:1 (protein: lipid molar) ratio, for a total concentration of s-Opa1 5×10^{-9} mol/ml (Ban et al., 2010;Zhang et al., 2020). In these studies interaction of s-Opa1 with CL is important for tubulation. Our asymmetric CL experiments observe tubulation even at lower concentrations. Due to the lack of CL on the outer (IMS facing) leaflet, we suspect that the major source of membrane for generating the tubes is the liposomes. Whether aspects of tubulation represent an intermediate in fusion will require further investigation. Future studies with asymmetric liposomes will also help discriminate s-Opa1 binding modes. In the asymmetric CL setting, s-Opa1 may interact with l-Opa1, and this heterotypic interaction might explain the observed increase in tethering.

In our previous studies under symmetric CL conditions, we observed fast and efficient membrane fusion upon addition of stoichiometric levels of s-Opa1 (Ge et al., 2020b). In this study, asymmetric CL distribution appears to stall progression to fusion, resulting in the growth of tubes. Further, addition of s-Opa1 dissociated tubes from the bilayer, suggesting a hetero-oligomeric l-Opa1: s-Opa1 interaction may play a role in association of these tubes with the supported bilayer. We did not observe any hemifusion events between tubes and supported bilayer, emphasizing the importance of CL in this leaflet for proceeding through fusion. The lack of stimulatory effect upon addition of s-Opa1 to a homotypic l-Opa1 arrangement also suggests s-Opa1 assembly (or interaction) with the supported bilayer plays a role in fusion.

The effects of membrane lipid composition and distribution on fusion involve the interplay of several physical properties. The kinetics of membrane fusion are influenced by the combination of membrane tension and membrane bending (Fan et al., 2016). Model membrane studies of

plasma membrane mimicking bilayers show line tension of a membrane plays a role in viral fusion, as positive curvature and membrane bending helps drive the two membranes to form a hemifusion stalk (Yang et al., 2016). Molecular dynamics simulations of symmetric CL bilayers show lateral heterogeneity contributes to bending of the bilayer. CL can be enriched in negatively curved regions and lateral heterogeneity within leaflets can lead to regions of positive curvature (Elias-Wolff et al., 2019). Our experimental system uses a polymer cushioned bilayer, which allows for a certain level of membrane fluctuation that may facilitate high-efficiency fusion. By depleting CL from the outer leaflet, the lateral heterogeneity of CL in the inner leaflet would be expected to be significantly less than in the symmetric bilayer, resulting in an altered membrane bending modulus that may contribute to slower pore opening than that observed in the asymmetric bilayer.

In this study, we explored CL asymmetry with 18:1 oleoyl-CL. The effects of CL modification are exciting areas for further investigation. Acyl chain composition, and the degree of CL saturation may vary dramatically in mitochondria (Kagan et al., 2014). At the IMM, mature CL is synthesized by a tafazzin from monolyso-CL (MLCL) (a three-tailed precursor) (Valianpour et al., 2005). During stress induced peroxidation, MLCL accumulates as a product of CL oxidation (Schlame and Xu, 2020). MLCL accumulation occurs in Barth syndrome (Valianpour et al., 2005). The three-acyl chain structure of MLCL (and its degradation products) are predicted to generate a “flatter” bilayer, less susceptible to curvature (Duncan, 2020). Cristae models indicate bilayers with high CL prefer highly curved regions and are prone to “defects” due to exposed hydrophobic regions. Supplementation with MLCL is predicted to decrease the likelihood for such “defects” (Boyd et al., 2018). In our experiments, we did indeed observe fewer defects in the asymmetric bilayers compared to symmetric bilayers. We hypothesize that lipid compositions sampled in these experiments may have properties common to those resulting from MLCL introduction. We anticipate our model membrane system will provide an ideal experimental platform for future systematic investigation of how lipid composition (in particular mitochondrial CL variants) affects protein and organelle function.

Conclusion

In this study we tested the effects of selectively removing CL from one leaflet of a model of the mitochondrial inner-membrane. We observed that simply removing CL from the inter membrane space facing leaflet resulted in interesting changes in membrane tethering, and stalled fusion. Furthermore, we observe formation of membrane tubes under these conditions. Low levels of CL are expected to be present in the IMS-facing leaflet under physiological conditions. These observations point to important conformations and assembly states of Opa1 regulated by the presence of CL. These studies also indicate many interesting membrane properties resulting from lipid asymmetry remain to be explored. The specific protein arrangements and membrane states of fusion are interesting questions for future integrated structural and biophysical studies.

References

Anand, R., Wai, T., Baker, M.J., Kladt, N., Schauss, A.C., Rugarli, E., and Langer, T. (2014). The i-AAA protease YME1L and OMA1 cleave OPA1 to balance mitochondrial fusion and fission. *J Cell Biol* 204**,** 919-929.

Ban, T., Heymann, J.A., Song, Z., Hinshaw, J.E., and Chan, D.C. (2010). OPA1 disease alleles causing dominant optic atrophy have defects in cardiolipin-stimulated GTP hydrolysis and membrane tubulation. *Hum Mol Genet* 19**,** 2113-2122.

Boyd, K.J., Alder, N.N., and May, E.R. (2017). Buckling Under Pressure: Curvature-Based Lipid Segregation and Stability Modulation in Cardiolipin-Containing Bilayers. *Langmuir* 33**,** 6937-6946.

Boyd, K.J., Alder, N.N., and May, E.R. (2018). Molecular Dynamics Analysis of Cardiolipin and Monolysocardiolipin on Bilayer Properties. *Biophys J* 114**,** 2116-2127.

Chan, D.C. (2020). Mitochondrial Dynamics and Its Involvement in Disease. *Annu Rev Pathol* 15**,** 235-259.

Chu, C.T., Ji, J., Dagda, R.K., Jiang, J.F., Tyurina, Y.Y., Kapralov, A.A., Tyurin, V.A., Yanamala, N., Shrivastava, I.H., Mohammadyani, D., Wang, K.Z.Q., Zhu, J., Klein-Seetharaman, J., Balasubramanian, K., Amoscato, A.A., Borisenko, G., Huang, Z., Gusdon, A.M., Cheikhi, A., Steer, E.K., Wang, R., Baty, C., Watkins, S., Bahar, I., Bayir, H., and Kagan, V.E. (2013). Cardiolipin externalization to the outer mitochondrial membrane acts as an elimination signal for mitophagy in neuronal cells. *Nat Cell Biol* 15**,** 1197-1205.

Cogliati, S., Enriquez, J.A., and Scorrano, L. (2016). Mitochondrial Cristae: Where Beauty Meets Functionality. *Trends Biochem Sci* 41**,** 261-273.

Del Dotto, V., Mishra, P., Vidoni, S., Fogazza, M., Maresca, A., Caporali, L., Mccaffery, J.M., Cappelletti, M., Baruffini, E., Lenaers, G., Chan, D., Rugolo, M., Carelli, V., and Zanna, C. (2017). OPA1 Isoforms in the Hierarchical Organization of Mitochondrial Functions. *Cell Rep* 19**,** 2557-2571.

Doktorova, M., Heberle, F.A., Eicher, B., Standaert, R.F., Katsaras, J., London, E., Pabst, G., and Marquardt, D. (2018). Preparation of asymmetric phospholipid vesicles for use as cell membrane models. *Nat Protoc* 13**,** 2086-2101.

Doktorova, M., Symons, J.L., and Levental, I. (2020). Structural and functional consequences of reversible lipid asymmetry in living membranes. *Nat Chem Biol* 16**,** 1321-1330.

Dudek, J. (2017). Role of Cardiolipin in Mitochondrial Signaling Pathways. *Front Cell Dev Biol* 5**,** 90.

Duncan, A.L. (2020). Monolysocardiolipin (MLCL) interactions with mitochondrial membrane proteins. *Biochem Soc Trans* 48**,** 993-1004.

Ehses, S., Raschke, I., Mancuso, G., Bernacchia, A., Geimer, S., Tondera, D., Martinou, J.C., Westermann, B., Rugarli, E.I., and Langer, T. (2009). Regulation of OPA1 processing and mitochondrial fusion by m-AAA protease isoenzymes and OMA1. *J Cell Biol* 187**,** 1023-1036.

Elias-Wolff, F., Linden, M., Lyubartsev, A.P., and Brandt, E.G. (2019). Curvature sensing by cardiolipin in simulated buckled membranes. *Soft Matter* 15**,** 792-802.

Faelber, K., Dietrich, L., Noel, J.K., Wollweber, F., Pfitzner, A.K., Muhleip, A., Sanchez, R., Kudryashev, M., Chiaruttini, N., Lilie, H., Schlegel, J., Rosenbaum, E., Hessenberger, M., Matthaeus, C., Kunz, S., Von Der Malsburg, A., Noe, F., Roux, A., Van Der Laan, M., Kuhlbrandt, W., and Daumke, O. (2019). Structure and assembly of the mitochondrial membrane remodelling GTPase Mgm1. *Nature* 571**,** 429-433.

Fan, Z.A., Tsang, K.Y., Chen, S.H., and Chen, Y.F. (2016). Revisit the Correlation between the Elastic Mechanics and Fusion of Lipid Membranes. *Sci Rep* 6**,** 31470.

Friedman, J.R., and Nunnari, J. (2014). Mitochondrial form and function. *Nature* 505**,** 335-343.

Gallet, P.F., Petit, J.M., Maftah, A., Zachowski, A., and Julien, R. (1997). Asymmetrical distribution of cardiolipin in yeast inner mitochondrial membrane triggered by carbon catabolite repression. *Biochem J* 324 (Pt 2)**,** 627-634.

Gao, S., and Hu, J. (2021). Mitochondrial Fusion: The Machineries In and Out. *Trends Cell Biol* 31**,** 62-74.

Ge, Y., Boopathy, S., Smith, A., and Chao, L.H. (2020a). A Model Membrane Platform for Reconstituting Mitochondrial Membrane Dynamics. *J Vis Exp*.

Ge, Y., Shi, X., Boopathy, S., Mcdonald, J., Smith, A.W., and Chao, L.H. (2020b). Two forms of Opa1 cooperate to complete fusion of the mitochondrial inner-membrane. *Elife* 9.

Giacomello, M., Pyakurel, A., Glytsou, C., and Scorrano, L. (2020). The cell biology of mitochondrial membrane dynamics. *Nat Rev Mol Cell Biol* 21**,** 204-224.

Harayama, T., and Riezman, H. (2018). Understanding the diversity of membrane lipid composition. *Nat Rev Mol Cell Biol* 19**,** 281-296.

Harb, J.S., Comte, J., and Gautheron, D.C. (1981). Asymmetrical orientation of phospholipids and their interactions with marker enzymes in pig heart mitochondrial inner membrane. *Archives of Biochemistry and Biophysics* 208**,** 305-318.

Horvath, S.E., and Daum, G. (2013). Lipids of mitochondria. *Prog Lipid Res* 52**,** 590-614.

Hossein, A., and Deserno, M. (2020). Spontaneous Curvature, Differential Stress, and Bending Modulus of Asymmetric Lipid Membranes. *Biophys J* 118**,** 624-642.

Hussain, N.F., Siegel, A.P., Ge, Y., Jordan, R., and Naumann, C.A. (2013). Bilayer asymmetry influences integrin sequestering in raft-mimicking lipid mixtures. *Biophys J* 104**,** 2212-2221.

Kagan, V.E., Chu, C.T., Tyurina, Y.Y., Cheikhi, A., and Bayir, H. (2014). Cardiolipin asymmetry, oxidation and signaling. *Chem Phys Lipids* 179**,** 64-69.

Kagan, V.E., Tyurina, Y.Y., Tyurin, V.A., Mohammadyani, D., Angeli, J.P., Baranov, S.V., Klein-Seetharaman, J., Friedlander, R.M., Mallampalli, R.K., Conrad, M., and Bayir, H. (2015). Cardiolipin signaling mechanisms: collapse of asymmetry and oxidation. *Antioxid Redox Signal* 22**,** 1667-1680.

Kondadi, A.K., Anand, R., and Reichert, A.S. (2020). Cristae Membrane Dynamics - A Paradigm Change. *Trends Cell Biol* 30**,** 923-936.

Kordower, J.H., Chu, Y., Hauser, R.A., Freeman, T.B., and Olanow, C.W. (2008). Lewy body-like pathology in long-term embryonic nigral transplants in Parkinson's disease. *Nat Med* 14**,** 504-506.

Krebs, J.J., Hauser, H., and Carafoli, E. (1979). Asymmetric distribution of phospholipids in the inner membrane of beef heart mitochondria. *J Biol Chem* 254**,** 5308-5316.

Kroemer, G., Galluzzi, L., and Brenner, C. (2007). Mitochondrial membrane permeabilization in cell death. *Physiol Rev* 87**,** 99-163.

Lemmin, T., Bovigny, C., Lancon, D., and Dal Peraro, M. (2013). Cardiolipin Models for Molecular Simulations of Bacterial and Mitochondrial Membranes. *J Chem Theory Comput* 9**,** 670-678.

Li, G., Kakuda, S., Suresh, P., Canals, D., Salamone, S., and London, E. (2019). Replacing plasma membrane outer leaflet lipids with exogenous lipid without damaging membrane integrity. *PLoS One* 14**,** e0223572.

London, E. (2019). Membrane Structure-Function Insights from Asymmetric Lipid Vesicles. *Acc Chem Res* 52**,** 2382-2391.

Lorent, J.H., Levental, K.R., Ganesan, L., Rivera-Longsworth, G., Sezgin, E., Doktorova, M., Lyman, E., and Levental, I. (2020). Plasma membranes are asymmetric in lipid unsaturation, packing and protein shape. *Nat Chem Biol* 16**,** 644-652.

Mcbride, H.M., Neuspiel, M., and Wasiak, S. (2006). Mitochondria: more than just a powerhouse. *Curr Biol* 16**,** R551-560.

Oemer, G., Koch, J., Wohlfarter, Y., Alam, M.T., Lackner, K., Sailer, S., Neumann, L., Lindner, H.H., Watschinger, K., Haltmeier, M., Werner, E.R., Zschocke, J., and Keller, M.A. (2020). Phospholipid Acyl Chain Diversity Controls the Tissue-Specific Assembly of Mitochondrial Cardiolipins. *Cell Rep* 30**,** 4281-4291 e4284.

Oemer, G., Lackner, K., Muigg, K., Krumschnabel, G., Watschinger, K., Sailer, S., Lindner, H., Gnaiger, E., Wortmann, S.B., Werner, E.R., Zschocke, J., and Keller, M.A. (2018). Molecular structural diversity of mitochondrial cardiolipins. *Proc Natl Acad Sci U S A* 115**,** 4158-4163.

Petit, J.M., Huet, O., Gallet, P.F., Maftah, A., Ratinaud, M.H., and Julien, R. (1994). Direct analysis and significance of cardiolipin transverse distribution in mitochondrial inner membranes. *Eur J Biochem* 220**,** 871-879.

Pizzuto, M., and Pelegrin, P. (2020). Cardiolipin in Immune Signaling and Cell Death. *Trends Cell Biol* 30**,** 892-903.

Ryan, T., Bamm, V.V., Stykel, M.G., Coackley, C.L., Humphries, K.M., Jamieson-Williams, R., Ambasudhan, R., Mosser, D.D., Lipton, S.A., Harauz, G., and Ryan, S.D. (2018). Cardiolipin exposure on the outer mitochondrial membrane modulates alpha-synuclein. *Nat Commun* 9**,** 817.

Schlame, M. (2008). Cardiolipin synthesis for the assembly of bacterial and mitochondrial membranes. *J Lipid Res* 49**,** 1607-1620.

Schlame, M., and Xu, Y. (2020). The Function of Tafazzin, a Mitochondrial Phospholipid-Lysophospholipid Acyltransferase. *J Mol Biol* 432**,** 5043-5051.

Song, Z., Chen, H., Fiket, M., Alexander, C., and Chan, D.C. (2007). OPA1 processing controls mitochondrial fusion and is regulated by mRNA splicing, membrane potential, and Yme1L. *J Cell Biol* 178**,** 749-755.

St Clair, J.W., Kakuda, S., and London, E. (2020). Induction of Ordered Lipid Raft Domain Formation by Loss of Lipid Asymmetry. *Biophys J* 119**,** 483-492.

Traïkia, M., Warschawski, D.E., Lambert, O., Rigaud, J.-L., and Devaux, P.F. (2002). Asymmetrical Membranes and Surface Tension. *Biophysical Journal* 83**,** 1443-1454.

Valianpour, F., Mitsakos, V., Schlemmer, D., Towbin, J.A., Taylor, J.M., Ekert, P.G., Thorburn, D.R., Munnich, A., Wanders, R.J., Barth, P.G., and Vaz, F.M. (2005). Monolysocardiolipins accumulate in Barth syndrome but do not lead to enhanced apoptosis. *J Lipid Res* 46**,** 1182-1195.

Van Laar, V.S., and Berman, S.B. (2009). Mitochondrial dynamics in Parkinson's disease. *Exp Neurol* 218**,** 247-256.

Wang, R., Mishra, P., Garbis, S.D., Moradian, A., Sweredoski, M.J., and Chan, D.C. (2021). Identification of new OPA1 cleavage site reveals that short isoforms regulate mitochondrial fusion. *Mol Biol Cell* 32**,** 157-168.

Wilson, B.A., Ramanathan, A., and Lopez, C.F. (2019). Cardiolipin-Dependent Properties of Model Mitochondrial Membranes from Molecular Simulations. *Biophys J* 117**,** 429-444.

Yan, L., Qi, Y., Ricketson, D., Li, L., Subramanian, K., Zhao, J., Yu, C., Wu, L., Sarsam, R., Wong, M., Lou, Z., Rao, Z., Nunnari, J., and Hu, J. (2020). Structural analysis of a

trimeric assembly of the mitochondrial dynamin-like GTPase Mgm1. *Proc Natl Acad Sci U S A* 117**,** 4061-4070.

Yang, S.T., Kiessling, V., and Tamm, L.K. (2016). Line tension at lipid phase boundaries as driving force for HIV fusion peptide-mediated fusion. *Nat Commun* 7**,** 11401.

Zhang, D., Zhang, Y., Ma, J., Zhu, C., Niu, T., Chen, W., Pang, X., Zhai, Y., and Sun, F. (2020). Cryo-EM structures of S-OPA1 reveal its interactions with membrane and changes upon nucleotide binding. *Elife* 9.

Fig. 1 Scheme for symmetric and asymmetric polymer-supported bilayers and evaluation of cardiolipin asymmetry by fluorescent anisotropy. Bilayers with symmetric and asymmetric CL distribution (A and D) show no difference in fluorescent emission intensity under EPI-fluorescence illumination (B and E). However, under polarized excitation ($P_{polarization}$) the intensity of the fluorescence intensity of P and S emission channels show significant difference (C and F). Fluorescent anisotropy measurements over time (G) show that bilayer asymmetry was stable and over a 48 hrs. Scale bar of each image: 10 μm. Data were collected from 4 bilayers with 5 random spot collected from each bilayer (ns, $P > 0.05$; *, $P \leq 0.05$; **, $P \leq 0.01$; ***, $P \leq 0.001$; ****, $P \leq 0.0001$).

Fig 2. Effect of cardiolipin distribution and membrane asymmetry on l-Opa1 mediated membrane tethering. We compared four conditions: no CL in the bilayer or proteoliposomes (Fig 2A i); 20 %(mol) CL symmetrically distributed in the bilayer, no CL in liposomes (Fig 2A ii); no CL in only the top leaflet of the bilayer, proteoliposomes with symmetric 20% CL (Fig 2A iii); 20% CL liposomes and bilayers, symmetrically distributed in both leaflets (Fig 2A iv). Scale bar: 10 μm. Data were collected from 3-5 independent experiments at 5~10 random positions. Statistical analyses done by t-test.

Fig 3. Effect of s-Opa1 on proteoliposome tethering addition to an asymmetric CL bilayer. 3A. In the presence of GTP, few l-Opa1 proteoliposomes are tethered to an asymmetric CL bilayer containing l-Opa1. 3B-E. Upon s-Opa1 addition, proteoliposome tethering increases significantly. Panels B-E show representative images varying l-Opa1 and s-Opa1 concentration shown in panel F as i-iv. Lipid tube formation indicated by red arrows. Scale bar of each image are 20 μm. Red arrows indicate tubular structures tethered to the bilayer. Corresponding quantification of the number of proteoliposomes tethered to the bilayer based on images from 3-5 different experiments from 10-20 random points from each experiment, data analyzed using t-test.

Fig. 4 Asymmetric distribution of CL determines the efficiency and kinetics of l-Opa1 mediated membrane lipid demixing (hemifusion) and content release. A. Schematic of the experiment. The lipid bilayer top leaflet was CL free, while the bottom leaflet contained 20 %(mol) CL. B. Example of hemifusion event without calcein release (scale bar = 1μm). The total process takes ~20 s. Fusion kinetics shown in E (Scale bar, 1μm), and calcein release can be recorded even after 30 seconds of total recording time. The total number of particles analyzed from 3~5 bilayers quantified in D (hemifusion) and G (fusion). Data were collected from 3 different experiments.

A

CL

TopFluor-CL

DOPC-PEG2000

Symmetric bilayer: both leaflet contains 15% cardiolipin and 0.1% TopFluor-CL

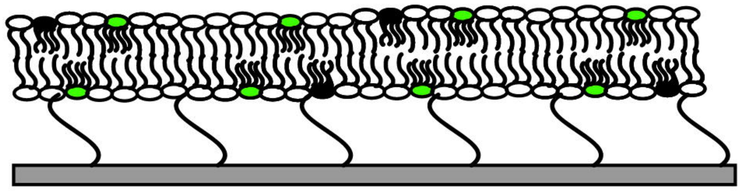

D

Asymmetric bilayer: bottom leaflet: 19.8% CL and 0.2% TopFluor-CL, Top leaflet: 10% CL

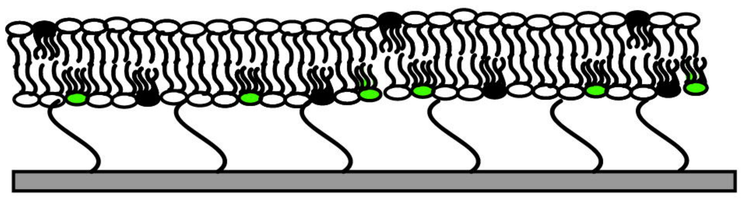

EPI

B

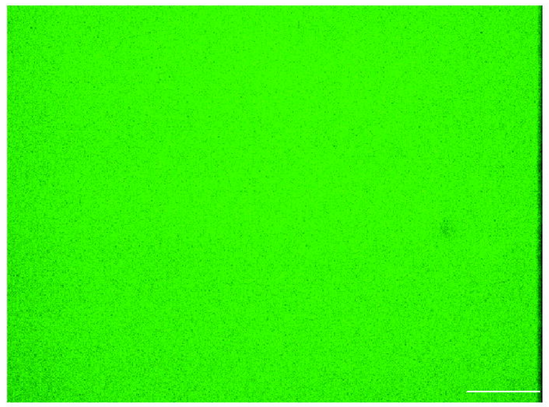

E

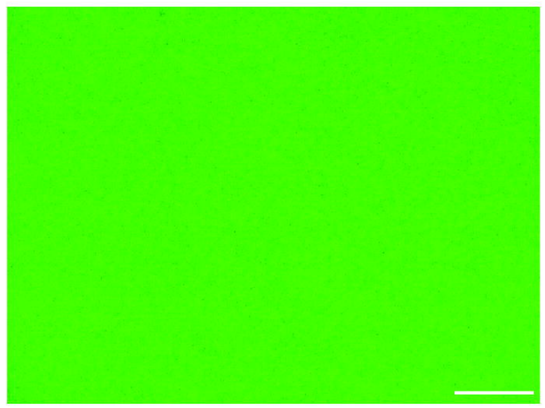

C

Fluorescent Anisotropy imaging (P-488 emission)

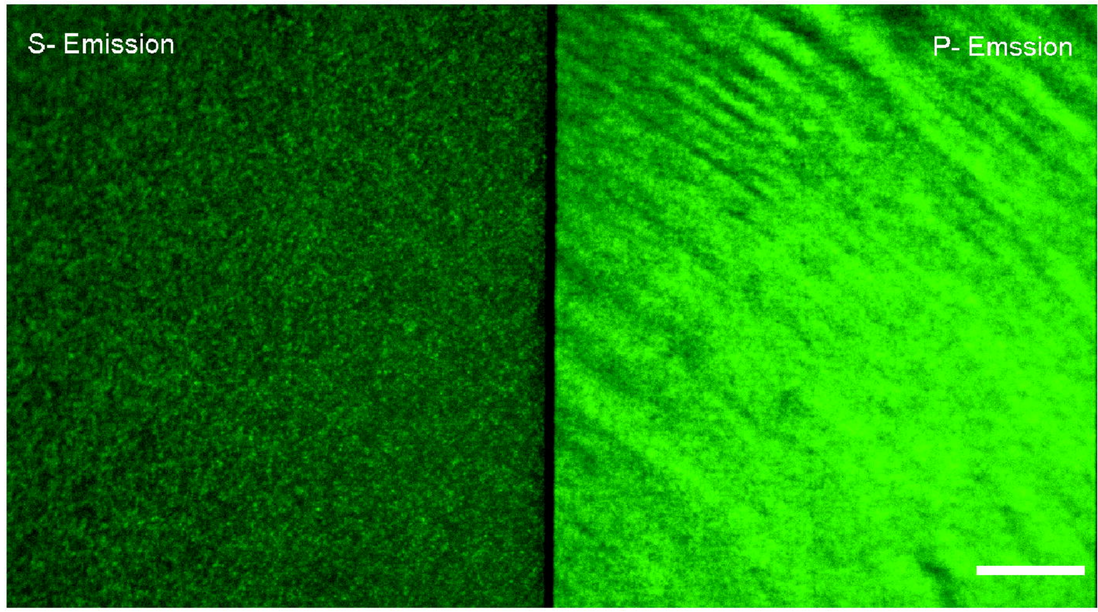

F

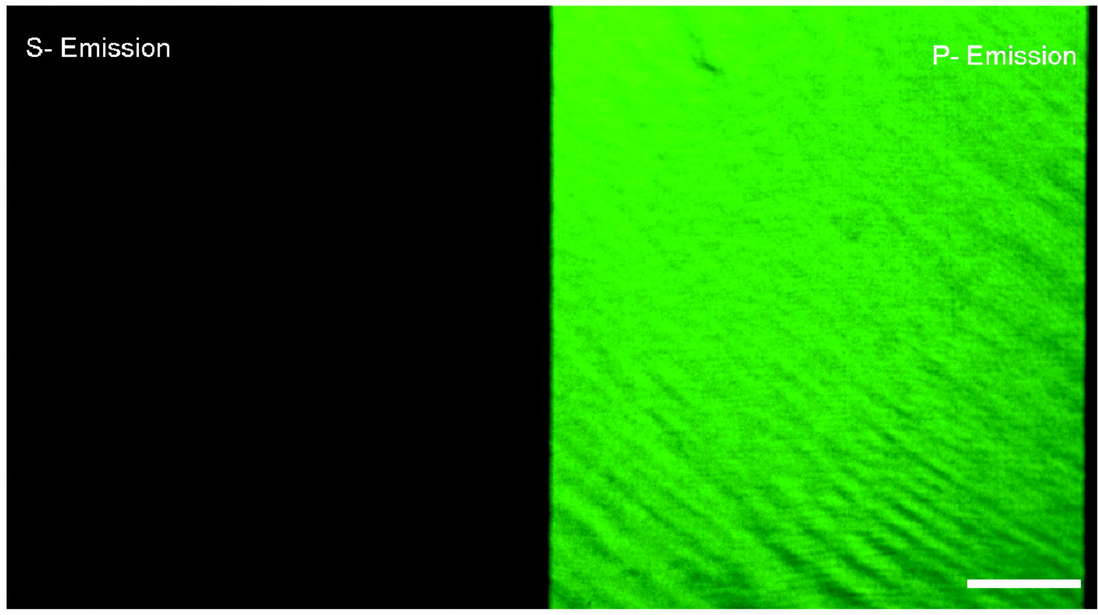

G

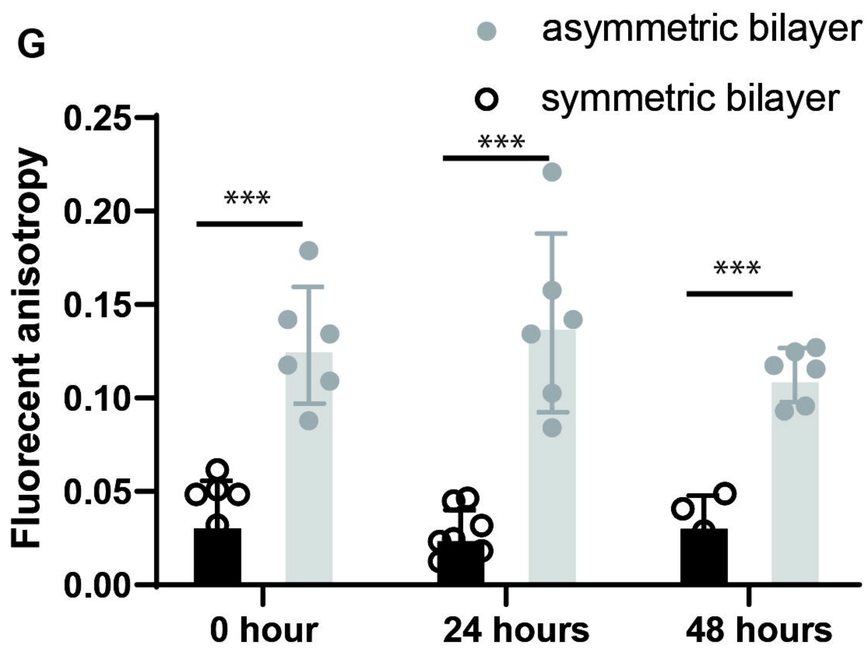

A

(i)

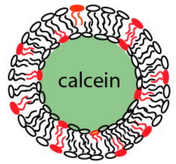

0% CL

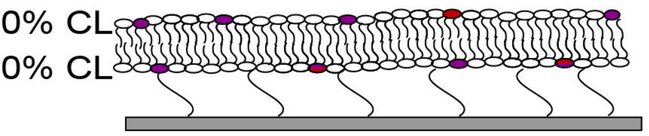

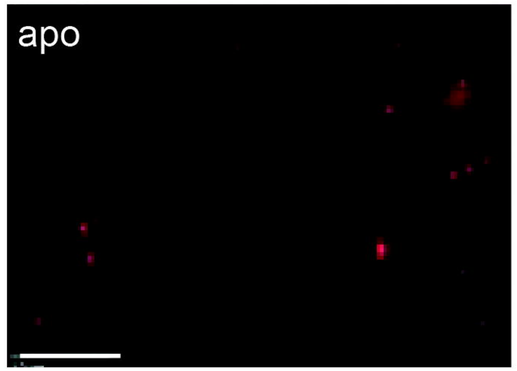

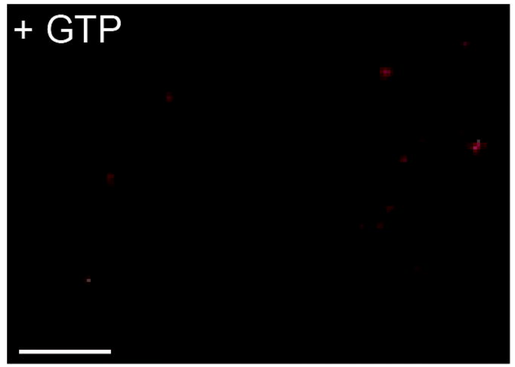

(ii)

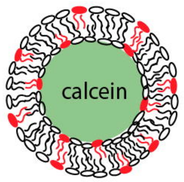

0% CL

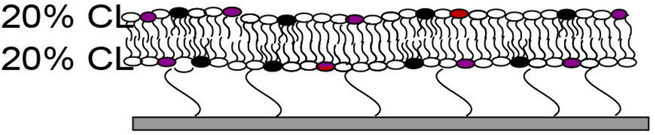

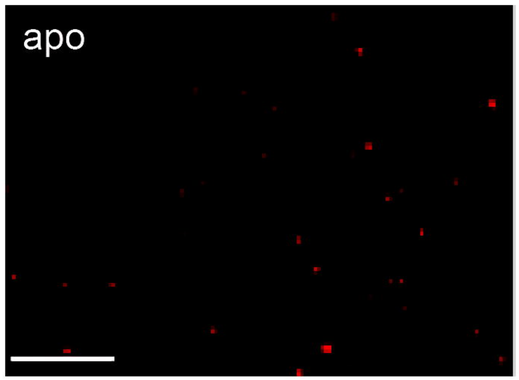

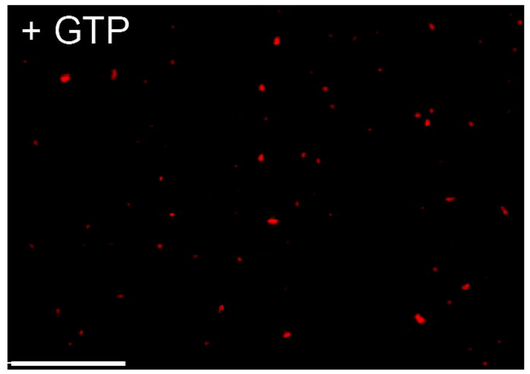

(iii)

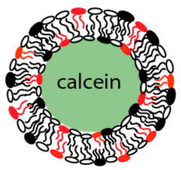

20% CL

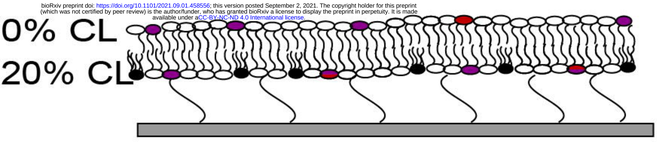

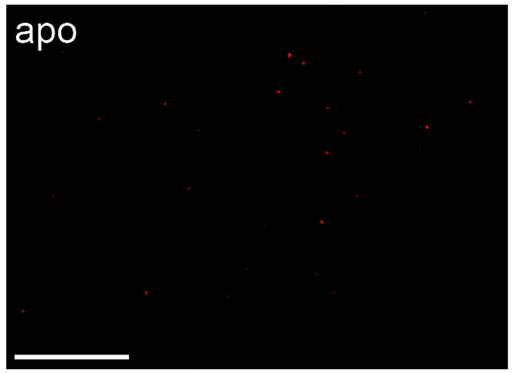

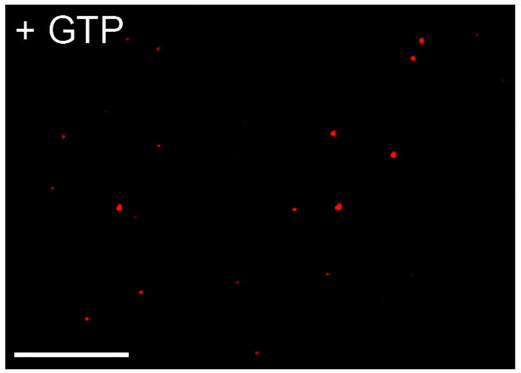

(iv)

20% CL

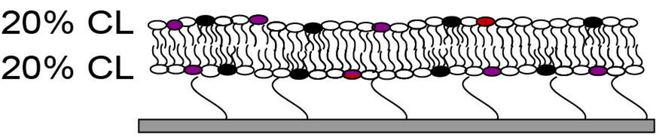

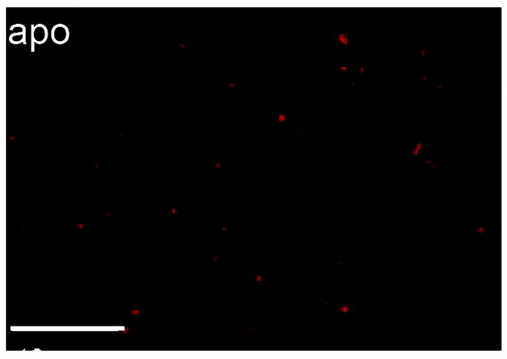

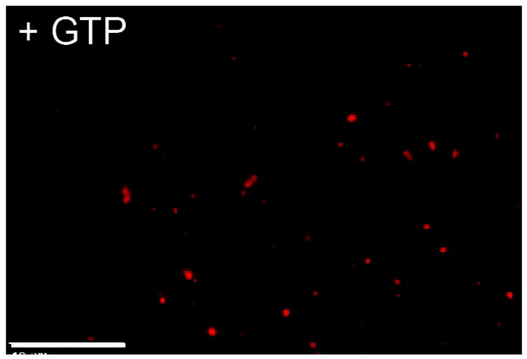

B

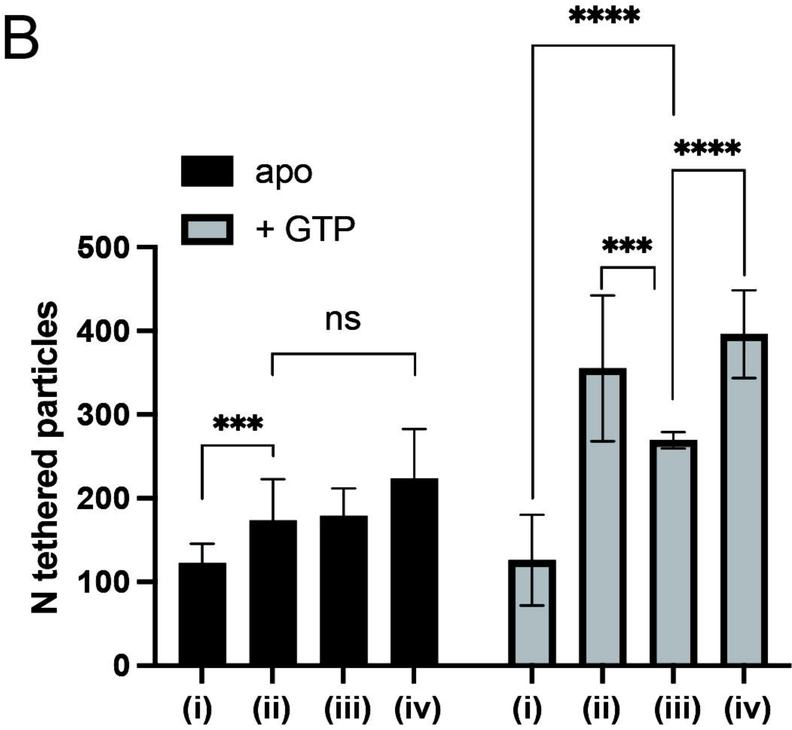

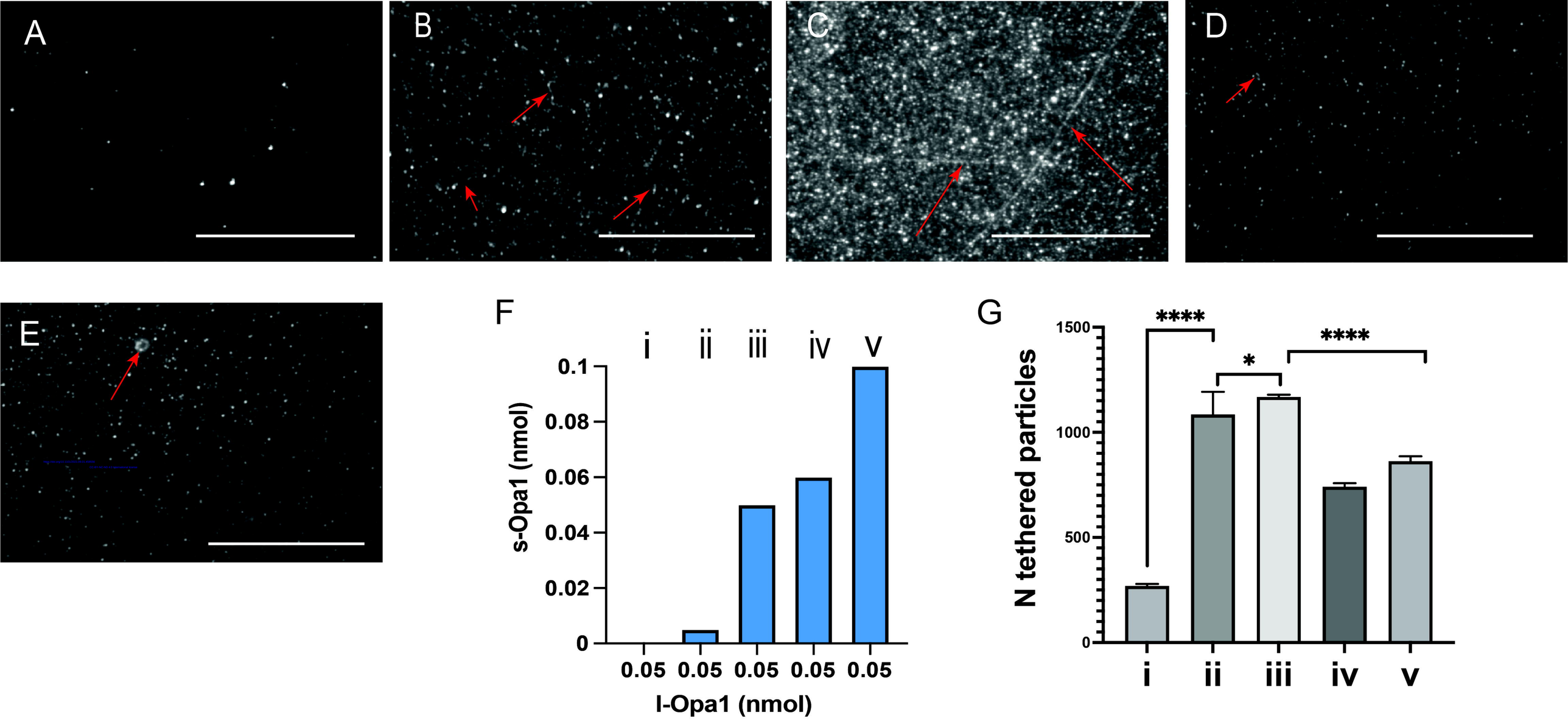
A
B
C
D
E
F
i
ii
iii
iv
v
0.1
0.08
0.06
0.04
0.02
0
s-Opa1 (nmol)
0.05 0.05 0.05 0.05 0.05
l-Opa1 (nmol)
G
****
*
****
1500
1000
500
0
N tethered particles
i
ii
iii
iv
v